

## Article

# Facile Synthesis of 3D Printed Tailored Electrode for 3-Monochloropropane-1,2-Diol (3-MCPD) Sensing

Farrah Aida Arris<sup>1,2</sup>, Denesh Mohan<sup>1,2</sup>  and Mohd Shaiful Sajab<sup>1,2,\*</sup> 

<sup>1</sup> Research Center for Sustainable Process Technology (CESPRO), Faculty of Engineering and Built Environment, Universiti Kebangsaan Malaysia, Bangi 43600, Selangor, Malaysia; farrahaidarris@gmail.com (F.A.A.); denesh.mohan@gmail.com (D.M.)

<sup>2</sup> Department of Chemical and Process Engineering, Faculty of Engineering and Built Environment, Universiti Kebangsaan Malaysia, Bangi 43600, Selangor, Malaysia

\* Correspondence: mohdshaiful@ukm.edu.my; Tel.: +60-3-8921-6425

**Abstract:** Additive manufacturing (AM) has allowed enormous advancement in technology and material development; thus, it requires attention in developing functionalized printed materials. AM can assist in efficiently manufacturing complex tailored electrodes for electrochemical sensing in the food industry. Herein, we used a commercial fused deposition modeling (FDM) filament of acrylonitrile butadiene styrene (ABS) for FDM 3D printing of a self-designed electrode with minimal time and cost compared to a commercial electrode. A graphene-based ABS conductive filament (ABS-G) was used to fabricate the conductive electrode in a dual-nozzle FDM 3D printer. The electrochemically conductive 3D printed electrode was characterized using cyclic voltammetry and tested against standard 3-monochloropropane-1,2-diol (3-MCPD) with known concentrations using an amperometric detection method. Results showed a basis for promising application to detect and quantify 3-MCPD, a food contaminant known for its carcinogenic potential. The fabrication of functionalized 3D printed polymer electrodes paves way for the development of complete 3D printable electrochemical sensors. Under optimal conditions, this newly synthesized electrochemical sensor exhibited sensitivity with a linear response range from  $6.61 \times 10^{-4}$  to  $2.30 \times 10^{-3}$   $\mu\text{g/mL}$  with an estimated limit of detection of  $3.30 \times 10^{-4}$   $\mu\text{g/mL}$  against 3-MCPD.

**Keywords:** additive manufacturing; electrodeposition; palm oil contaminant; cyclic voltammetry; 3-monochloropropane-1,2-diol (3-MCPD); zero-valent iron (ZVI)



**Citation:** Arris, F.A.; Mohan, D.; Sajab, M.S. Facile Synthesis of 3D Printed Tailored Electrode for 3-Monochloropropane-1,2-Diol (3-MCPD) Sensing. *Micromachines* **2022**, *13*, 383. <https://doi.org/10.3390/mi13030383>

Academic Editor: Aiqun Liu

Received: 4 February 2022

Accepted: 24 February 2022

Published: 27 February 2022

**Publisher's Note:** MDPI stays neutral with regard to jurisdictional claims in published maps and institutional affiliations.



**Copyright:** © 2022 by the authors. Licensee MDPI, Basel, Switzerland. This article is an open access article distributed under the terms and conditions of the Creative Commons Attribution (CC BY) license (<https://creativecommons.org/licenses/by/4.0/>).

## 1. Introduction

AM technology is developing rapidly with various types of AM techniques due to the ease of product manufacturing and production of customized products [1–3]. FDM is the most common AM technology used for fabrication because of the inexpensive FDM 3D printer and materials [4]. The ABS material for FDM 3D printing has been extensively evaluated for polymer-based applications, but its use has been limited in electrochemical sensing applications due to its electrical insulating properties [5]. The advancement in FDM 3D printing polymer modification with conductive fillers such as graphene and carbon black could pave way for the fabrication of customized portable and complex sensing devices [6–9]. Further functionalization of the conductive 3D printed electrodes with gold (Au) and silver chloride (AgCl) has been achieved for commercial electrochemical sensing [6,10,11]. This development could be further investigated for sensor application in the food industry with functionalized materials for the detection of various types of analytes such as mycotoxins and 3-monochloropropane-1,2-diol (3-MCPD) [12].

In 2016, the European Food Safety Authority (EFSA) started to evaluate the severity of consuming foods containing 3-MCPD, which is an organic chemical compound found in processed foods such as refined vegetable oils, breads, and soy sauce [13]. The glycerol-based contaminant was concluded to be potentially carcinogenic according to toxicological

data from tests performed on rats, imposing danger to humans upon consumption beyond tolerable limits [14]. Among refined vegetable oils, palm oil was reported to have the highest 3-MCPD content [15–17]. The formation of 3-MCPD was contributed by the presence of several precursors such as acylglycerols and chloride-containing compounds, with the combination of other factors such as conditions during the oil refining process, which applies elevated temperatures up to 260 °C and the addition of acid-activated bleaching during the deodorization stage [16–23].

Due to the potential risk of 3-MCPD, a safe intake limit was introduced to ensure that palm oil is safe for human consumption. The intake limit of 3-MCPD was set to 2 µg/kg body weight per day by the FAO/WHO Expert Committee on Food Additives, while a 0.02 mg/kg regulatory limit was set for hydrolyzed vegetable protein and soy sauce by the European Union [24]. To comply with the 3-MCPD safe limit, reliable methods of detection and quantification must be standardized and used. The most frequently used method to detect and quantify 3-MCPD content is gas chromatography–mass spectrometry (GC–MS). GC–MS, however, requires the oil sample to be prepared by a derivatization process for the 3-MCPD to be readable. The oil sample preparation also requires a significant amount of solvent to allow for liquid extraction. GC–MS also needs to be conducted in the laboratory due to the mobility limitation of the instrument and requires skilled personnel to perform the test [25]. On average, GC–MS results can be produced in at least 2 h; therefore, it is considered a time-consuming method. The cost of GC–MS is also not cheap; thus, with the increasing demand to test more frequently for accuracy, it is not economical. Therefore, there is a need to establish a simple, rapid, mobile, and reliable analytical method to quantify 3-MCPD, especially for on-site measurement. One approach is to produce a portable electrochemical sensing device that is able to detect and measure the occurrence of 3-MPCD, as well as the amount at any point during the refining process.

Zero-valent iron (ZVI) is often referred to as an environmentally friendly material, which has been used extensively in wastewater treatment to remediate and remove highly toxic elements such as arsenic(III) in groundwater and supercapacitor electrodes [26,27]. ZVI is also effective for the degradation of halogenated solvents such as chlorinated compounds and is suspected to be able to react with chlorinated solvents, a characteristic that might be useful for targeting contaminated palm oil [28]. The electrochemical deposition method is used to coat or deposit nanomaterials in specific suspensions or solutions by applying the concept of donating electrons to ions [29]. The selection of the electrodeposition method can help to ensure the further reduction of iron in suspension and provide enhanced adhesion of ZVI onto the 3D printed electrode substrate. In this study, a 3D printed acrylonitrile butadiene styrene (ABS)-insulated conductive graphene (ABS-G) electrode was fabricated using a commercial FDM filament. ZVI was tested for deposition onto the newly fabricated 3D printed ABS-G electrode using the drop-casting method, followed by electrodeposition to increase and improve the ZVI adhesion. Next, the 3D printed ABS-G was electrochemically analyzed and calibrated to determine its feasibility for detecting 3-MCPD.

## 2. Materials and Methods

### 2.1. Chemicals and Reagents

Commercially available ABS green filament and ABS conductive filament (graphene-based) of 1.75 mm were procured for FDM 3D printing. Iron(II) sulfate heptahydrate ( $\text{FeSO}_4 \cdot 7\text{H}_2\text{O}$ ), sodium borohydride ( $\text{NaBH}_4$ ), potassium chloride (KCl), potassium ferricyanide ( $\text{K}_3[\text{Fe}(\text{CN})_6]$ ), sodium hydroxide (NaOH), and 3-MCPD were purchased from Sigma-Aldrich (M) Sdn. Bhd. (Selangor, Malaysia). All analytical reagents used in this work were prepared without further refinement and used as obtained. Deionized (DI) water was used as solvent throughout this work.

## 2.2. Instrumentation and Methods

Electrochemical characterization of the newly fabricated 3D printed ABS-G electrode was performed using cyclic voltammetry (CV) on a 910 PSTAT Mini (Metrohm, Herisau, Switzerland) and a three-electrode configuration consisting of the newly 3D printed ABS-G as the working electrode (WE), platinum (Pt) as the counter electrode (CE), and silver/silver chloride (Ag/AgCl) as the reference electrode (RE) in 0.05 M ferricyanide solution as the electrolyte. The electrochemical characterization was performed in order to understand the electron-transfer capabilities of the sensor.

Field-emission scanning electron microscopy (FE-SEM) with energy-dispersive X-rays spectroscopy (EDX) (Merlin Compact, Zeiss Pvt. Ltd., Oberkochen, Germany) was used to characterize the surface morphology and to provide elemental analysis of the deposited ZVI onto the 3D printed ABS-G electrode. The functional groups of the 3D printed electrode were determined using attenuated total reflectance Fourier-transform infrared (ATR-FTIR) spectroscopy (ALPHA FTIR Spectrometer, Bruker, Billerica, MA, USA) in the range of 4000 to 500  $\text{cm}^{-1}$  at a resolution of 1  $\text{cm}^{-1}$ .

## 2.3. Fabrication of 3D Printed ABS-G Electrode

The desired electrode design was modeled using computer-aided design (CAD) software and sliced to a G-code file through slicer software (Ultimaker Cura 4.7, Geldermalsen, Netherlands). The composite electrodes were then 3D printed using a three-axis FDM 3D printer with a dual nozzle (Flashforge Creator 3, Jinhua, China). The printing profile was fixed on the basis of findings from a previous study (nozzle diameter: 0.4 mm, printing temperature: 255 °C, layer height: 0.15 mm; infill percentage: 80%; infill pattern: 45° lines; print speed: 60 mm/s) [30].

## 2.4. Preparation and Deposition of Zero-Valent Iron (ZVI)

Zero-valent iron (ZVI) was synthesized according to [31] with minor modification.  $\text{FeSO}_4 \cdot 7\text{H}_2\text{O}$  was diluted in ethanol and DI water, and then reduced using  $\text{NaBH}_4$  to form a greenish-black suspension of ZVI. Deposition of ZVI was performed by drop casting 50  $\mu\text{L}$  of ZVI suspension onto the 3D printed ABS-G electrode surface, which was allowed to dry. Next, the modified 3D printed ABS-G electrode was electrochemically treated and deposited in ZVI suspension using CV mode for five scan cycles to further assist in the reduction of ZVI, as well as the adhesion of nanomaterial onto the electrode surface.

## 2.5. Electrochemical Characterization and Calibration of ABS-G and ABS-G/ZVI

In order to better understand the electroactive capability of the bare and modified electrode to transfer electrons, CV was performed in 0.05 M of  $\text{K}_3[\text{Fe}(\text{CN})_6]$  as an electrochemical redox solution using a three-electrode configuration. Calibration against a known 3-MCPD standard solution was executed using amperometric detection in order to understand the feasibility of the sensor to detect and quantify 3-MCPD. The method was performed by adding a fixed volume of 3-MCPD standard in DI water within a fixed interval of time, and the current change was observed over time as a response to the spiked concentration of 3-MCPD in the sample. A scan rate of 100 mV/s was used for the CV experiment unless otherwise stated.

# 3. Results and Discussion

## 3.1. 3D Printing of Electrochemically Conductive Electrode

CAD software was utilized in designing an electrically insulated electrode with ABS in the outer layer, which can be seen in Figure 1a. The G-code comprising an optimized printing profile compatible with a dual-nozzle 3D printer (see Figure 1b) was obtained for FDM 3D printing. The dual-material 3D printed electrode shown in Figure 1c could be fabricated within a short time at low cost, showing the potential of 3D printing for mass commercialization. The automated printing process with high precision using a 0.4 mm diameter nozzle was able to print the dual-material electrode within 58 min. Further

development of a conductive filament with higher conductivity will further enhance the development of 3D printed electronics, as the filament can be used directly in the fabrication of electronic circuits, capacitors, and transducers.

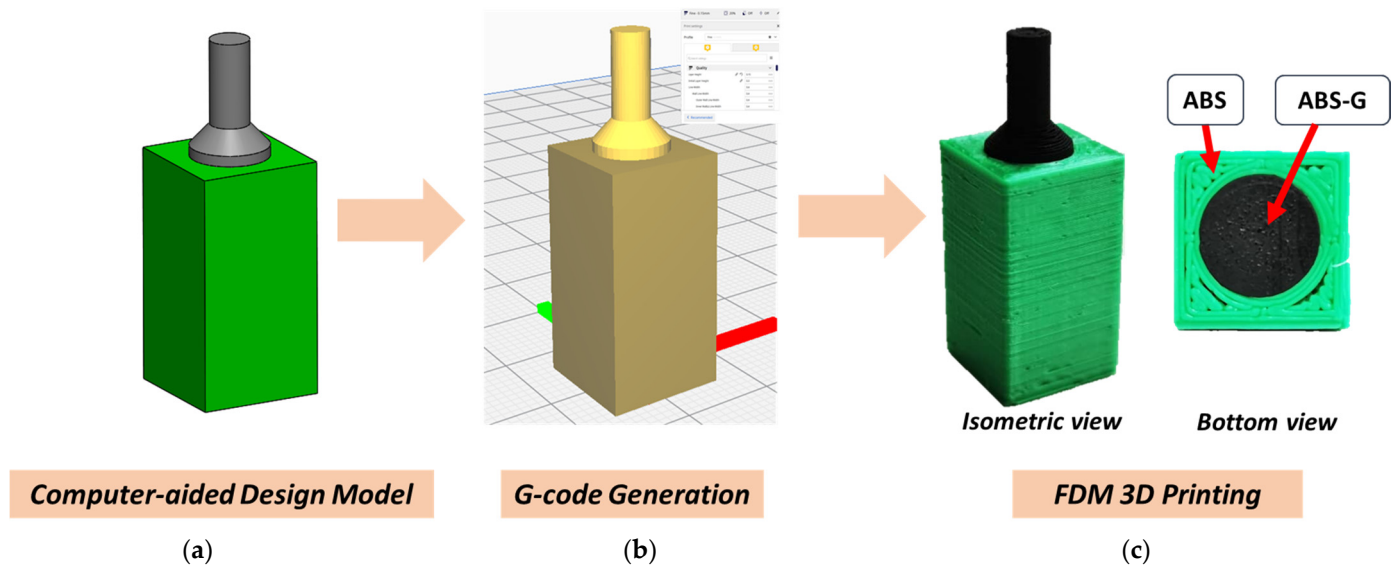
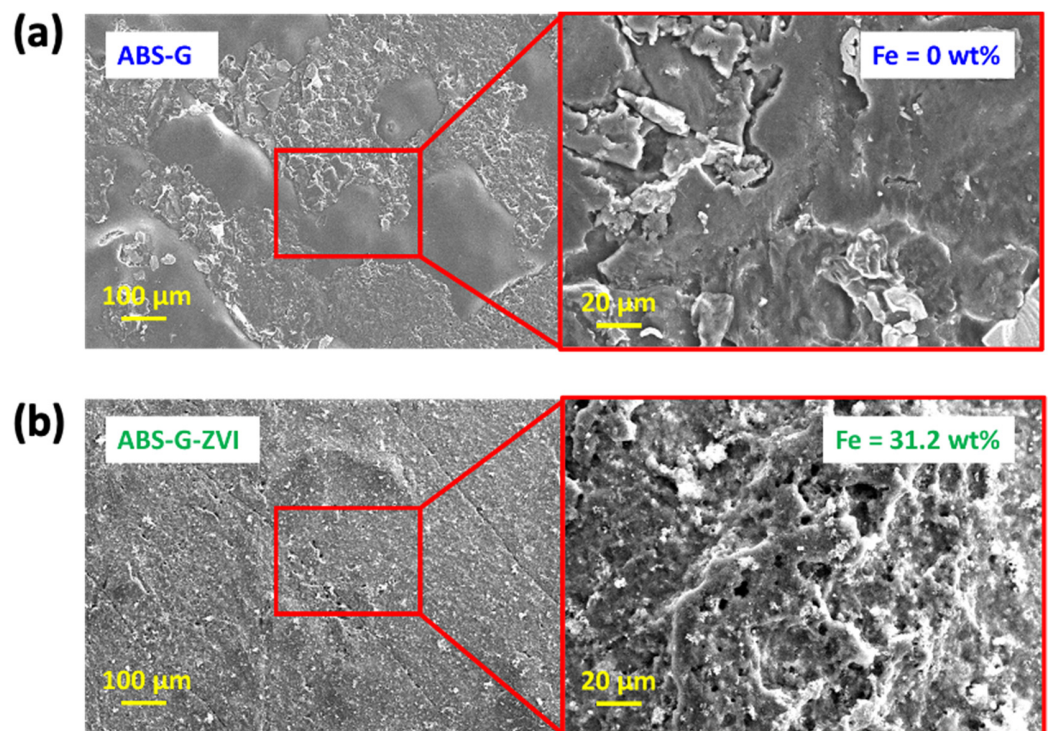


**Figure 1.** Fabrication process of 3D printed composite electrode. (a) Computer-aided design model, (b) G-code generation, (c) FDM 3D printing.

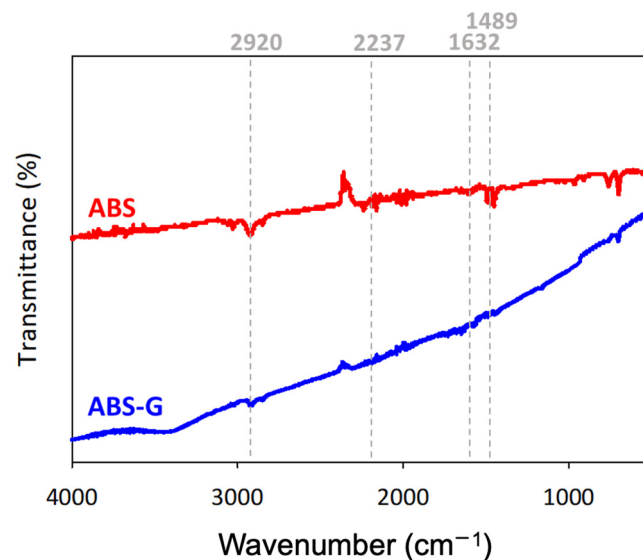
### 3.2. Characterization of 3D Printed ABS-G and ABS-G/ZVI Electrodes

Figure 2a presents the FE-SEM image of the 3D printed ABS-G electrode morphological surface, where the absence of iron nanoparticles was observed. Figure 2b, on the other hand, presents the FE-SEM image of the 3D printed ABS-G electrode with ZVI deposited onto its surface, which can be seen from the agglomeration of iron nanoparticles. Further elemental composition analysis using EDX showed an estimation of 31.2 wt.% of iron nanoparticles successfully deposited onto the 3D printed ABS-G electrode. The improvement in surface roughness after ZVI deposition can also enable better adhesion of nanomaterials to improve analyte detection. The deposited ZVI can also enhance the surface area-to-volume ratio for the available sites to perform electrochemical detection of 3-MCPD.

Figure 3 shows the FTIR spectra for the ABS and ABS-G electrode. The FTIR spectrum of ABS (see Figure 3) shows aliphatic stretching at  $2920\text{ cm}^{-1}$ , acrylonitrile at  $2237\text{ cm}^{-1}$ , C=C of butadiene at  $1632\text{ cm}^{-1}$ , and the styrene unit at  $1489\text{ cm}^{-1}$  [12]. The graphene content in the ABS-G filament, reported to be 10% with respect to the functional groups of ABS-G, was the same compared to ABS, indicating that graphene did not change the chemical structure of ABS [32]. Absorption peaks at  $1489$  and  $1632\text{ cm}^{-1}$  belong to the nitrile group and double bonds of butadiene and double bonds of styrene in ABS polymers [33]. The absorption peak at  $2920\text{ cm}^{-1}$  refers to the aliphatic and aromatic C–H bonds in ABS [34].



**Figure 2.** (a) Field-emission scanning electron microscope (FE-SEM) and EDX images of the 3D printed ABS-G electrode; (b) FE-SEM and EDX images of the 3D printed ABS-G electrode with electrochemically deposited ZVI.



**Figure 3.** Fourier-transform infrared (FTIR) of 3D printed filaments.

### 3.3. Electrochemical Characterization of 3D Printed ABS-G and ABS-G/ZVI Electrodes

Figure 4a shows the CV curves of the 3D printed ABS, 3D printed ABS-G, and 3D printed ABS-G with electrodeposited ZVI electrodes measured in 0.05 M  $K_3[Fe(CN)_6]$  solution at a scan rate of 0.1 V/s tested within the potential range of 0.2 to 1.0 V (vs. Ag/AgCl). With just ABS, negligible electron-transfer capability was observed, indicating the inability of the ABS polymer to perform electrochemistry, whereas conductive ABS exhibited enhanced current detection. This was attributed to the graphene filler incorporation, which conferred the attractive properties of graphene, which has a single atomic layer of 2D carbon and exhibits excellent electron mobility, and graphite, with few or more layers of graphene.

The electron mobility of graphene in ABS allows the material to be utilized as a transducer for sensor fabrication. Despite the ABS-G electrode depicting the capability of electron transfer, the conductivity was not feasible to be utilized directly in electrochemical sensing [35,36]. Thus, electrodeposition of ZVI onto 3D printed ABS-G was conducted to further enhance the redox capability of the 3D electrode, corresponding to 0.05 M ferricyanide as the electrolyte, as can be seen in Figure 4.

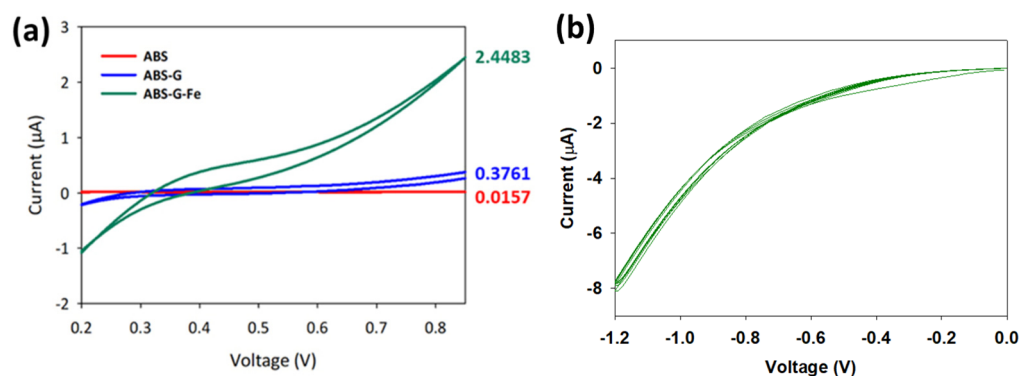


**Figure 4.** (a) CV curves of ABS, ABS-G, and ABS-G with electrodeposited ZVI; (b) electrodeposition of ZVI for five scan cycles using CV mode.

The ZVI suspension was electrodeposited onto the substrate 3D printed ABS-G electrode as shown in Figure 4b for five scan cycles. The electrodeposition process was performed in CV mode, with a running voltage from 0 V to  $-1.2$  V for five scan cycles. During the process, a thin layer of ZVI was electrochemically deposited onto the 3D printed ABS-G electrode surface as shown in the FE-SEM and EDX images in Figure 2b. Upon successful completion of the electrodeposition process, the 3D printed ABS-G/ZVI electrode was fabricated and ready for application.

### 3.4. Calibration in 3-MCPD Using ZVI-3D Printed ABS-G Electrode

In order to test the performance of the 3D printed ABS-G electrodeposited with ZVI (denoted as ABS-G/ZVI electrode) in detecting 3-MCPD, calibration was performed using amperometric method. The calibration was conducted in 0.3 M NaOH solution at a fixed potential of 1.3 V, with the addition of 10  $\mu$ L of 3-MCPD standard suspension at 300 s time intervals. The detection of 3-MCPD was achieved through a combination of surface adsorption and electron transfer happening in the redox solution, resulting in the current output measured.

As shown in Figure 5a, at  $t = 0$ , the current measured was due to the movement of electrons in 0.3 M NaOH. Upon the first addition of 10  $\mu$ L of 3-MCPD at  $t = 300$  s, the redox peak current started to change direction, possibly due to the adjustment of 3-MCPD in the NaOH solution. Further addition of 10  $\mu$ L of 3-MCPD at  $t = 600$  s resulted in a decrease in the peak current as the 3-MCPD concentration increased. This decreasing peak current trend showed that the 3D printed ABS-G/ZVI sensor successfully detected 3-MCPD in the 0.3 M NaOH, with similar trends reported by [33,34,37]. It is important to determine the incubation time between each addition of 3-MCPD standard suspension prior to performing amperometry to ensure a more reflective and better peak current measured. The incubation time for each experiment varies according to the setting. For instance, 3-MCPD detection using imprinted *p*-aminothiophenol (*p*-ATP-AuNP/GCE) in soy sauce requires at least 6 min incubation time before the measurement of peak current using the DPV method [38]. The calibration plot of current measured according to the corresponding 3-MCPD concentration ( $R^2$  of 0.9539) in Figure 5b exhibits a linear response range from  $6.61 \times 10^{-4}$  to  $2.30 \times 10^{-3}$   $\mu$ g/mL with an estimated limit of detection of  $3.30 \times 10^{-4}$   $\mu$ g/mL against 3-MCPD detection. A comparison of past reports related to electrochemical detection of 3-MCPD mostly in soy sauce can be seen in Table 1 below.

Most past reports utilized gold nanomaterials and molecularly imprinted polymers (MIP) to enhance the sensitivity and selectivity of the fabricated sensor in detection 3-MCPD against other analytes. None of the studies utilized electrodeposited ZVI as the transducer nanomaterial, and none of the studies reported on 3-MCPD sensing in edible oils.

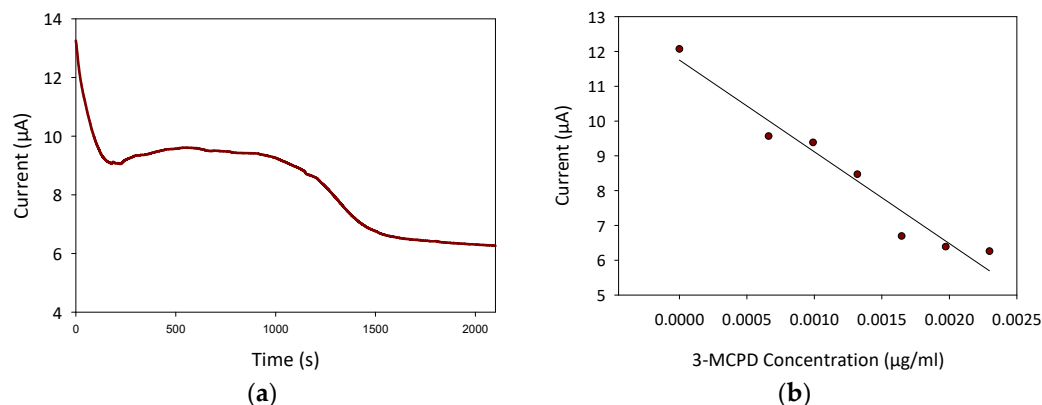


**Figure 5.** (a) Amperometric curves of ABS, ABS-G, and ABS-G with electrodeposited ZVI; (b) calibration plot of current measured versus 3-MCPD concentration ( $R^2 = 0.9539$ ).

**Table 1.** Comparison between electrochemical 3-MCPD sensors based on past reports.

Electrode	Method of Detection	Linear Range	Lower Detection Limit	Reference
Glassy carbon electrode (GCE)/nanoporous gold (NPG)/molecularly imprinted polymer (MIP)	Differential pulse voltammetry (DPV)	$10^{-16}$ to $10^{-7}$ mol/L	$3.5 \times 10^{-17}$ mol/L	[39]
Glassy carbon electrode (GCE)/hemoglobin immobilized with magnetic molecularly imprinted nanoparticles (Hb-MMIPs NPs)	Differential pulse voltammetry (DPV)	1.0 to 160.0 mg/L	0.25 mg/L	[40]
Gold (Au)/cysteine-coated silver nanoparticles (Cys-AgNPs)	Differential pulse voltammetry (DPV)	2.5 to 200 ng/mL	2.4 ng/mL	[41]
Glassy carbon electrode (GCE)/carboxylated multi-wall carbon nanotubes (MWCNT)/metal-organic framework (MOF-199)	Differential pulse voltammetry (DPV)	$1.0 \times 10^{-9}$ to $1.0 \times 10^{-5}$ mol/L	$4.3 \times 10^{-10}$ mol/L	[37]
GCE/AuN/p-ATP	Differential pulse voltammetry (DPV)	$1.0 \times 10^{-17}$ to $1.0 \times 10^{-13}$ mol/L	$3.8 \times 10^{-18}$ mol/L	[38]

The preliminary results reveal a promising alternative platform for 3-MCPD detection, which can be performed outside the laboratory, with cheaper and faster results compared to the current method using GC-MS. GC-MS requires trained personnel; therefore, an alternative method that is simpler and more user-friendly should be developed, as the identification of 3-MCPD is currently attracting great attention. Furthermore, due to the complexity of 3-MCPD that can appear in both esterified and free forms, further electrode modification is needed in order to improve the detection sensitivity and selectivity against other contaminants, especially when tested in a complex environment such as edible oil. Depending on the target application, the detection and measurement of 3-MCPD in free or esterified form might require further sample preparation to be performed prior to the detection of 3-MCPD as the targeted analyte. For instance, an indirect traditional method of detecting 3-MCPD using GC-MS requires the sample to undergo transesterification to release 3-MCPD from its esterified form. Therefore, if the target is to detect and measure total 3-MCPD content, a similar transesterification process might be required prior to electrochemical analysis.

One of the improvements that can be achieved for this 3D printed electrode for 3-MCPD detection is related to its stability against harsh and complex environments, e.g., when testing in hot edible oil. Improvements must also be made on the sensitivity of the sensor by manipulating a nanocomposite of ZVI and polymers as the transducer layer. This can also help to preserve the shelf-life of the sensor for storage purposes. In a nutshell, developing a rapid test kit (RTK) for 3-MCPD detection in households represents a future direction in electrochemical sensing and should be made accessible to all, affordable, and easy to use.

#### 4. Conclusions

The recent advancement in 3D printing technology for sensor fabrication has enabled analyte detection in various environments using electrochemical sensing, which is a simpler and cheaper production method. The 3D printing approach was applied by incorporating conductive fillers in the form of graphene into commercially available polymers of ABS. Successful adhesion of ZVI nanomaterial was also performed using the electrodeposition method, which further enhanced the redox capability of the tailored design 3D printed electrode. In this study, a 3D printed electrode using ABS with functionalized graphene was fabricated and tested for ZVI nanomaterial adhesion and 3-MCPD detection as the primary transducer element for future modification in electrochemical sensing applications, e.g., rapid and on-site detection of 3-MCPD in its free form. Further research to improve the stability, sensitivity, and selectivity of the fabricated 3D printed electrode to detect 3-MCPD in real life has to be achieved by improving the transducer and detection layers of the electrode sensor. The utilization of a nanocomposite with polymers can also help to enhance the 3-MCPD detection limit and selectivity. Successful calibration against 3-MCPD showed a promising opportunity in detecting this processed food contaminant, paving the way toward fabricating an electrochemical sensor with rapid, portable, and cheap sensing capabilities for 3-MCPD as the targeted analyte. Developing a 3-MCPD RTK for households can also help to improve the awareness of food contaminants and reduce the health risk of consuming food with contaminants above the tolerable daily intake (TDI).

**Author Contributions:** Conceptualization, M.S.S.; methodology, F.A.A. and D.M.; validation, F.A.A.; formal analysis, F.A.A.; writing—original draft preparation, F.A.A. and D.M.; writing—review and editing, F.A.A. and M.S.S.; funding acquisition, M.S.S. All authors have read and agreed to the published version of the manuscript.

**Funding:** This research was funded by Universiti Kebangsaan Malaysia, grant numbers [GUP-2021-018] and [TAP-K021080].

**Conflicts of Interest:** The authors declare no conflict of interest.

#### References

1. Mohan, D.; Sajab, M.S.; Bakarudin, S.B.; Bin Roslan, R.; Kaco, H. 3D Printed Polyurethane Reinforced Graphene Nanoplatelets. *Mater. Sci. Forum* **2021**, *1025*, 47–52. [[CrossRef](#)]
2. Mohan, D.; Sajab, M.S.; Kaco, H.; Bakarudin, S.B.; Noor, A.M. 3D Printing of UV-Curable Polyurethane Incorporated with Surface-Grafted Nanocellulose. *Nanomaterials* **2019**, *9*, 1726. [[CrossRef](#)]
3. Mohan, D.; Khairullah, N.F.; How, Y.P.; Sajab, M.S.; Kaco, H. 3D Printed Laminated CaCO<sub>3</sub>-Nanocellulose Films as Controlled-Release 5-Fluorouracil. *Polymers* **2020**, *12*, 986. [[CrossRef](#)] [[PubMed](#)]
4. Mohan, D.; Teong, Z.K.; Bakir, A.N.; Sajab, M.S.; Kaco, H. Extending Cellulose-Based Polymers Application in Additive Manufacturing Technology: A Review of Recent Approaches. *Polymers* **2020**, *12*, 1876. [[CrossRef](#)] [[PubMed](#)]
5. Singh, R.; Sandhu, G.S.; Penna, R.; Farina, I. Investigations for thermal and electrical conductivity of ABS-graphene blended prototypes. *Materials* **2017**, *10*, 881. [[CrossRef](#)] [[PubMed](#)]
6. Foo, C.Y.; Lim, H.N.; Mahdi, M.A.; Wahid, M.H.; Huang, N.M. Three-dimensional printed electrode and its novel applications in electronic devices. *Sci. Rep.* **2018**, *8*, 1–11. [[CrossRef](#)]
7. Jayanth, N.; Senthil, P. Application of 3D printed ABS based conductive carbon black composite sensor in void fraction measurement. *Compos. Part B Eng.* **2019**, *159*, 224–230.

8. Wirth, D.M.; Sheaff, M.J.; Waldman, J.V.; Symcox, M.P.; Whitehead, H.D.; Sharp, J.D.; Doerfler, J.R.; Lamar, A.A.; Leblanc, G. Electrolysis activation of fused-filament-fabrication 3D-printed electrodes for electrochemical and spectroelectrochemical analysis. *Anal. Chem.* **2019**, *91*, 5553–5557. [[CrossRef](#)]
9. Flowers, P.F.; Reyes, C.; Ye, S.; Kim, M.J.; Wiley, B.J. 3D printing electronic components and circuits with conductive thermoplastic filament. *Addit. Manuf.* **2017**, *18*, 156–163. [[CrossRef](#)]
10. Rohaizad, N.; Mayorga-Martinez, C.C.; Novotný, F.; Webster, R.D.; Pumera, M. 3D-printed Ag/AgCl pseudo-reference electrodes. *Electrochem. Commun.* **2019**, *103*, 104–108. [[CrossRef](#)]
11. Cardoso, R.M.; Mendonça, D.M.H.; Silva, W.P.; Silva, M.N.T.; Nossol, E.; da Silva, R.A.B.; Richter, E.M.; Muñoz, R.A.A. 3D printing for electroanalysis: From multiuse electrochemical cells to sensors. *Anal. Chim. Acta* **2018**, *1033*, 49–57. [[CrossRef](#)] [[PubMed](#)]
12. Nasir, M.Z.M.; Novotný, F.; Alduhaish, O.; Pumera, M. 3D-printed electrodes for the detection of mycotoxins in food. *Electrochem. Commun.* **2020**, *115*, 106735. [[CrossRef](#)]
13. European Food Safety Authority. Analysis of occurrence of 3-monochloropropane-1, 2-diol (3-MCPD) in food in Europe in the years 2009–2011 and preliminary exposure assessment. *EFSA J.* **2013**, *11*, 3381. [[CrossRef](#)]
14. Abraham, K.; Appel, K.E.; Berger-Preiss, E.; Apel, E.; Gerling, S.; Mielke, H.; Creutzenberg, O.; Lampen, A. Relative oral bioavailability of 3-MCPD from 3-MCPD fatty acid esters in rats. *Arch. Toxicol.* **2013**, *87*, 649–659. [[CrossRef](#)] [[PubMed](#)]
15. Ariseto, A.P.; Marcolino, P.F.C.; Vicente, E. Determination of 3-monochloropropane-1,2-diol fatty acid esters in Brazilian vegetable oils and fats by an in-house validated method. *Food Addit. Contam. A* **2014**, *31*, 1385–1392. [[CrossRef](#)] [[PubMed](#)]
16. Pudel, F.; Benecke, P.; Fehling, P.; Freudenstein, A.; Matthäus, B.; Schwaf, A. On the necessity of edible oil refining and possible sources of 3-MCPD and glycidyl esters. *Eur. J. Lipid Sci. Technol.* **2011**, *113*, 368–373. [[CrossRef](#)]
17. Arris, F.A.; Thai, V.T.S.; Manan, W.N.; Sajab, M.S. A Revisit to the Formation and Mitigation of 3-Chloropropane-1,2-Diol in Palm Oil Production. *Foods* **2020**, *9*, 1769. [[CrossRef](#)] [[PubMed](#)]
18. Destailats, F.; Craft, B.D.; Sandoz, L.; Nagy, K. Formation mechanisms of Monochloropropanediol (MCPD) fatty acid diesters in refined palm (*Elaeis guineensis*) oil and related fractions. *Food Addit. Contam. Part A Chem. Anal. Control. Expo. Risk Assess* **2012**, *29*, 29–37. [[CrossRef](#)] [[PubMed](#)]
19. Nagy, K.; Sandoz, L.; Craft, B.D.; Destailats, F. Mass-defect filtering of isotope signatures to reveal the source of chlorinated palm oil contaminants. *Food Addit. Contam. Part A Chem. Anal. Control. Expo. Risk Assess* **2011**, *28*, 1492–1500. [[CrossRef](#)]
20. Šmidrkal, J.; Tesárová, M.; Hrádková, I.; Berčíková, M.; Adamčíková, A.; Filip, V. Mechanism of formation of 3-chloropropane-1,2-diol (3-MCPD) esters under conditions of the vegetable oil refining. *Food Chem.* **2016**, *211*, 124–129. [[CrossRef](#)]
21. Freudenstein, A.; Weking, J.; Matthäus, B. Influence of precursors on the formation of 3-MCPD and glycidyl esters in a model oil under simulated deodorization conditions. *Eur. J. Lipid Sci. Technol.* **2013**, *115*, 286–294. [[CrossRef](#)]
22. Shimizu, M.; Weitkamp, P.; Vosmann, K.; Matthäus, B. Influence of chloride and glycidyl-ester on the generation of 3-MCPD- and glycidyl-esters. *Eur. J. Lipid Sci. Technol.* **2013**, *115*, 735–739. [[CrossRef](#)]
23. Tiong, S.H.; Saparin, N.; Teh, H.F.; Ng, T.L.M.; bin Zain, M.M.Z.; Neoh, B.K.; Md Noor, A.; Tan, C.P.; Lai, O.M.; Appleton, D.R. Natural Organochlorines as Precursors of 3-Monochloropropanediol Esters in Vegetable Oils. *J. Agric. Food Chem.* **2018**, *66*, 999–1007. [[CrossRef](#)] [[PubMed](#)]
24. Weißhaar, R. Fatty acid esters of 3-MCPD: Overview of occurrence and exposure estimates. *Eur. J. Lipid Sci. Technol.* **2011**, *113*, 304–308. [[CrossRef](#)]
25. Dininova, V.; Svejkska, B.; Dolezal, M.; Velisek, J. Determination of free and bound 3-chloropropane-1,2-diol by gas chromatography with mass spectrometric detection using deuterated 3-chloropropane-1,2-diol as internal standard. *Czech. J. Food Sci.* **2005**, *22*, 182–189. [[CrossRef](#)]
26. Fu, F.; Dionysiou, D.D.; Liu, H. The use of zero-valent iron for groundwater remediation and wastewater treatment: A review. *J. Hazard. Mater.* **2014**, *267*, 194–205. [[CrossRef](#)]
27. Liu, H.; Wang, Q.; Wang, C.; Li, X.Z. Electron efficiency of zero-valent iron for groundwater remediation and wastewater treatment. *Chem. Eng. J.* **2013**, *215*, 90–95. [[CrossRef](#)]
28. Cook, S.M. *Assessing the Use and Application of Zero-Valent Iron Nanoparticle Technology for Remediation at Contaminated Sites*; Jackson State University: Washington, DC, USA, 2009.
29. Li, C.; Iqbal, M.; Lin, J.; Luo, X.; Jiang, B.; Malgras, V.; Wu, K.C.W.; Kim, J. Electrochemical deposition: An advanced approach for templated synthesis of nanoporous metal architectures. *Acc. Chem. Res.* **2018**, *51*, 1764–1773. [[CrossRef](#)] [[PubMed](#)]
30. Mohan, D.; Bakir, A.N.; Sajab, M.S.; Bakarudin, S.B.; Mansor, N.N.; Roslan, R.; Kaco, H. Homogeneous distribution of lignin/graphene fillers with enhanced interlayer adhesion for 3D printing filament. *Polym. Compos.* **2021**, *42*, 2408–2421. [[CrossRef](#)]
31. Arris, F.A.; Manan, W.N.; Kaco, H.; Shaffie, A.H.; Sajab, M.S. Electrochemical Characterization of Graphite-Zero-Valent Iron for 3-Monochloropropane-1,2-Diol (3-MCPD) Detection. *Mater. Sci. Forum* **2021**, *1025*, 20–25. [[CrossRef](#)]
32. Jiang, G.; Yang, T.; Xu, J.; Tao, D.; Luo, C.; Wang, C.; Dong, Q.; Wang, Y. Investigation into hydroxypropyl-methylcellulose-reinforced polylactide composites for fused deposition modelling. *Ind. Crops Prod.* **2020**, *146*, 112174. [[CrossRef](#)]
33. Heo, C.; Moon, H.G.; Yoon, C.S.; Chang, J.H. ABS nanocomposite films based on functionalized-graphene sheets. *J. Appl. Polym. Sci.* **2012**, *124*, 4663–4670. [[CrossRef](#)]

34. Fahmy, T.; Sarhan, A.; Elsayed, I.A.; Abdelwahed, H.G. Optical Properties of Poly (Vinyl Chloride-co-Vinyl Acetate-co-2-Hydroxypropyl Acrylate)/(Acrylonitrile-Butadiene-Styrene) Blends. *Int. J. Eng. Res.* **2018**, *11*, 1405–1415.
35. Adhikari, D.; Mukai, M.; Kubota, K.; Kai, T.; Kaneko, N.; Araki, K.S.; Kubo, M. Degradation of Bioplastics in Soil and Their Degradation Effects on Environmental Microorganisms. *J. Agric. Chem. Environ.* **2016**, *05*, 23–34. [[CrossRef](#)]
36. Shrestha, A.; van-Eerten Jansen, M.C.A.A.; Acharya, B. Biodegradation of bioplastic using anaerobic digestion at retention time as per industrial biogas plant and international norms. *Sustainability* **2020**, *12*, 4231. [[CrossRef](#)]
37. Han, S.; Ding, Y.; Teng, F.; Yao, A.; Leng, Q. Determination of chloropropanol with an imprinted electrochemical sensor based on multi-walled carbon nanotubes/metal-organic framework composites. *RSC Adv.* **2021**, *11*, 18468–18475. [[CrossRef](#)]
38. Sun, X.; Zhang, L.; Zhang, H.; Qian, H.; Zhang, Y.; Tang, L.; Li, Z. Development and application of 3-chloro-1,2-propandiol electrochemical sensor based on a polyaminothiophenol modified molecularly imprinted film. *J. Agric. Food Chem.* **2014**, *62*, 4552–4557. [[CrossRef](#)] [[PubMed](#)]
39. Cheng, W.; Zhang, Q.; Wu, D.; Yang, Y.; Zhang, Y.; Tang, X. A facile electrochemical method for rapid determination of 3-chloropropane-1,2-diol in soy sauce based on nanoporous gold capped with molecularly imprinted polymer. *Food Control* **2022**, *134*, 108750. [[CrossRef](#)]
40. Yuan, Y.; Wang, J.; Ni, X.; Cao, Y. A biosensor based on hemoglobin immobilized with magnetic molecularly imprinted nanoparticles and modified on a magnetic electrode for direct electrochemical determination of 3-chloro-1, 2-propandiol. *J. Electroanal. Chem.* **2019**, *834*, 233–240. [[CrossRef](#)]
41. Martin, A.A.; Fodjo, E.K.; Eric-Simon, Z.V.; Gu, Z.; Yang, G.; Albert, T.; Kong, C.; Wang, H.F. Cys-AgNPs modified gold electrode as an ultrasensitive electrochemical sensor for the detection of 3-chloropropane-1, 2-diol. *Arab. J. Chem.* **2021**, *14*, 103319. [[CrossRef](#)]